Supplementary Information

Localized Interfacial Activation Effect within Interconnected Porous Photothermal Matrix to Promote Solar-driven Water Evaporation

Jingjing Zhang, Jiaxiang Ma, Dongmei Liu, Dongqing Liu, Yu Han, Ying Xu, Fuyi Cui, Wei Wang

Table of Contents

Materials and Methods

Chemicals. Graphite flakes were provided by ASHINE Graphene RD Center, China. Sodium nitrate, sulfuric acid, potassium permanganate, and hydrochloric acid (37% solution) were purchased from Tianjin Guangfu Fine Chemical Institute, China. Hydrogen peroxide (30% solution) were purchased from Tianjin Kermel Chemical Reagent Co. LTD. Dopamine (DA) and Tris(hydroxymethyl)methylaminomethane (THAM) were purchased from Aladdin Industrial Inc. Shanghai, China. Ethanol was purchased from Xilong Chemical Co., Ltd, China.

Preparation of IPPM under alkaline condition. During the preparation of the photothermal matrix under alkaline condition, the GO (1.5 mg mL^{-1}) and DA (0.5 mg mL^{-1}) were mixed thoroughly in the Tris-HCl buffer solution (pH=8.5) and then the mixture was heated in water bath at 95 ^{o}C for 12 h. The obtained assembly was washed by DI water for several times to remove the residual salt ions. Some samples were frozen with liquid nitrogen and dried in a freeze drier (FD-1C-50, Beijing Boyikang Experimental Instrument Co. LTD) before usage for characterizations.

Molecular dynamics simulation. The interaction between interfacial water molecules and the IPPM interface, rGO (model of IPPM deducting PDA) as well as pure water were simulated by Molecular dynamics simulations (Forcite module in Materials studio 2017). The sizes of the three models were all the same (10.3 nm ×5.1 nm) and the elemental atomic ratio of the IPPM model was corresponding to that of the actual XPS element atomic ratio. The interfacial water layer consists of 1600 water molecules had the initial size of 10.3 nm ×5.1 nm × 0.9 nm. A vacuum layer of 150 Å was added in the model system where a fixed graphite sheet baffle was set around 75 Å to prevent water molecules from running to the bottom of the system. The total calculation time of the system was 5 ns in the NVT ensemble at 298.15 K (Nose thermostat) adopting the compass force field. The step size is 2.5 ps. The electrostatic interactions were computed using the Ewald summation method. The van der Waals interactions were computed using an atom-based summation method (a cutoff distance of 10.5 Å). The last 2.5 ns of the NVT simulation was used for the analysis. Before molecular dynamics calculations, the models should be relaxed enough to eliminate unreasonable contacts between atoms. In addition, the electrostatic potential diagram of the simplified rGO-PDA model was obtained by the dmol3 module in Materials studio.

Solar evaporation efficiency calculation and desalination capacity test.

The energy efficiency (η) of the IPPM was calculated as follows:

$$\eta = mh_T/qC_{opt} \quad (1)$$

$$h_T = h_S + h_L \quad (2)$$

in which m is the evaporation rate deducting the dark evaporation value (0.16 kg m^{-2} h^{-1}) of IPPM, h_T is the total equivalent vaporization enthalpy of the water in IPPM, including the sensible heat h_S of the water in which the system reaches equilibrium

temperature and the latent heat h_L of the water-vapor phase transition at the IPPM interface. q is the solar irradiation power of one sun (1 kW m^{-2}), and C_{opt} refers to the optical concentration on the surface of the photothermal matrix. Here, the sensible enthalpy change h_S is 51.2 J g^{-1} when the equilibrium temperature of water reached 39.1 ^oC (Fig. S13). Since the evaporation enthalpy of water molecules at the IPPM interface is 1500 J g^{-1} at room temperature, the latent heat of IPPM is 1472.5 J g^{-1} when the vapor temperature is 37.2 ^oC according to the relationship between the heat of vaporization of water and the temperature. Hence, the photothermal conversion efficiency of IPPM is calculated to be 86.3% according to formula.

To investigate the desalination capacity of the IPPM, the real seawater was collected from South China Sea, China. Different solutions of $CuCl_2$, $CdCl_2$, $NiCl_2$ and $ZnCl_2$ were used to investigate the removal of heavy metal ions. The escaped water from the solution containing metal ions during photothermal evaporation was collected for water quality testing, in which the evaporation device was placed in a closed transparent glass container for the collection of condensed water. The salinities of the elements contained in the raw water and the distilled water were measured by inductively coupled plasma spectroscopy (ICP–OES, OPTIMA 5300 DV, PerkinElmer Instrument).

Comsol simulation of water transport in IPPMs. Numerical simulations were conducted by COMSOL Multiphysics 4.5. The models for water transport in IPPMs (IPPM and IPPM-48 h) were established based on multi-physics coupling including non-isothermal flow and surface to surface radiative heat transfer. The models with the size of 100 μm ×100 μm were comprised of porous substrate and water, ignoring the complexity caused by deformation during irradiation. According to the experimental data, it was assumed that the environment temperature was set to 298.15 K and the simulated solar irradiation was 1 kW m^{-2}. The average water transport rates on the bottom side of the models were viewed as being identical to the actual average water loss rates of the photothermal matrixes (0.61 μm s^{-1} for IPPM, 0.33 μm s^{-1} for IPPM-48 h). Consequently, the surficial water loss rates in the two models were 0.69 and 0.39 μm s^{-1}, respectively, by simulation calculation, which were close to the actual value.

Supporting results

S1. XRD data and TEM images of GO.

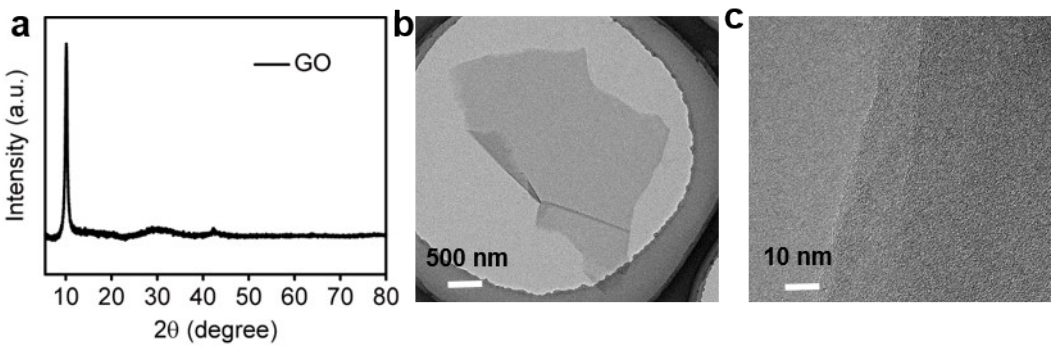

Fig. S1 XRD data and TEM images of GO.

S2. Photographs of GO/DA solution during acid-assembly.

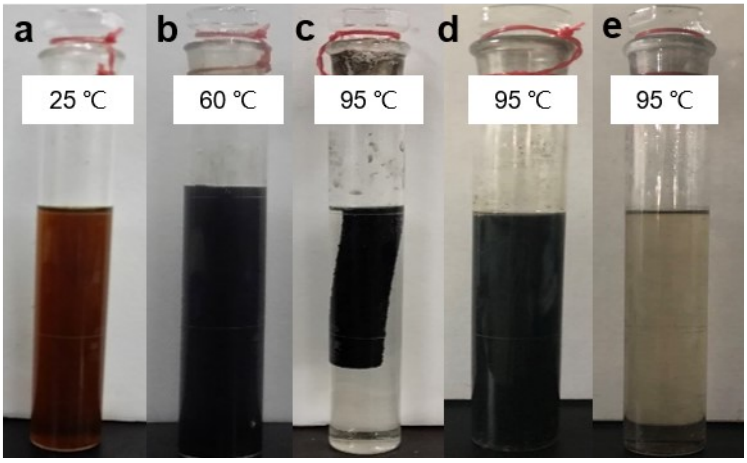

Fig. S2 Photographs of the GO&DA mixed solutions at (a) 25 ^{o}C, (b) 60 ^{o}Cand (c) 95 ^{o}C after heating for 12 hours. (d) Photograph of acidic GO solution after heating for 12 hours. (e) Photograph of acidic DA solution after heating for 12 hours.

S3. Water contact angle of IPPM.

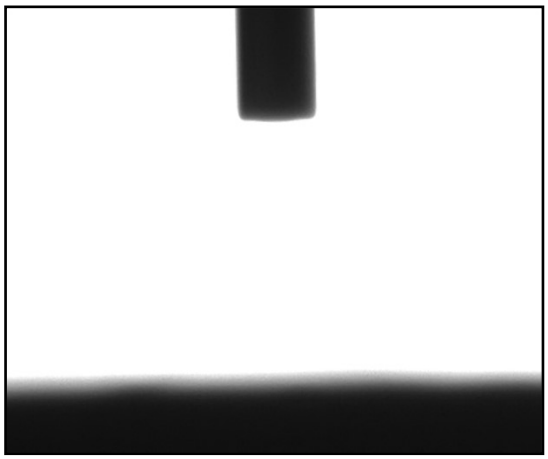

Fig. S3 Water contact angle of IPPM.

S4. Surface morphology characterization of IPPM.

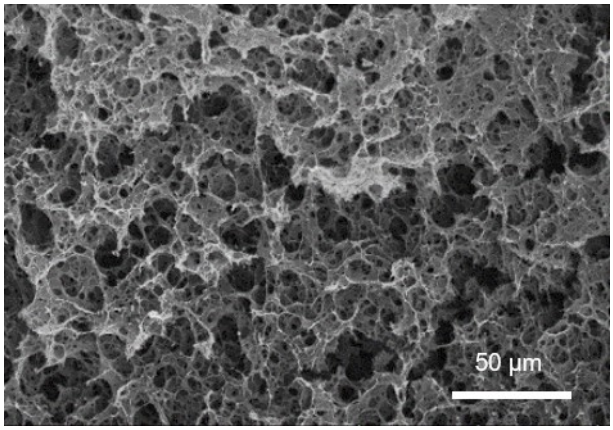

Fig. S4 Low-magnification SEM image of IPPM.

S5. EDS mapping characterization.

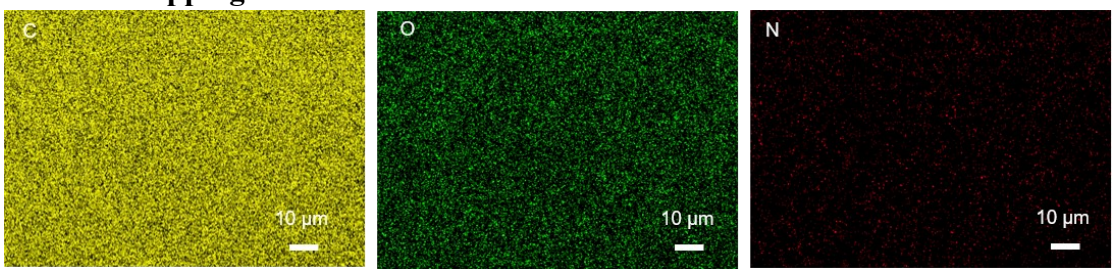

Fig. 5 EDS mapping of IPPM.

S6. Surface morphology of hydrogel prepared by alkaline-assembly process.

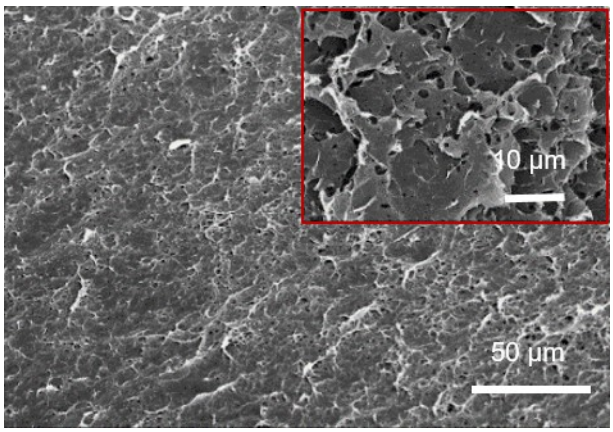

Fig. S6 SEM image of hydrogel prepared under alkaline condition.

S7. XPS analysis of IPPM.

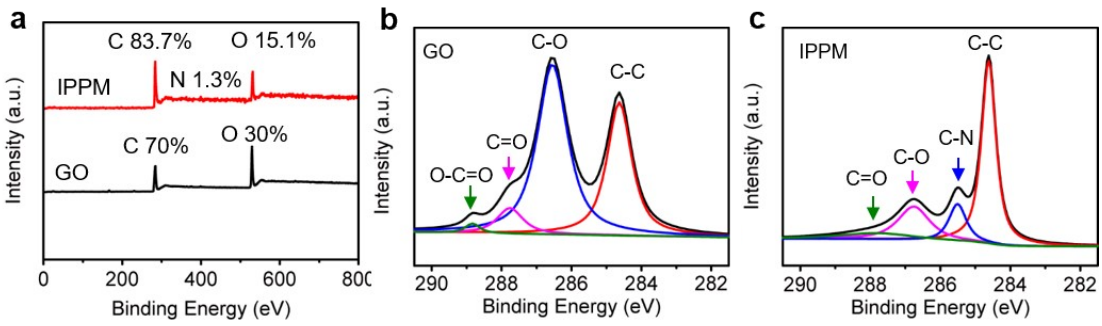

Fig. S7 (a) Element component analysis of IPPM and GO. XPS spectrum of (b) GO and (c) IPPM.

S8. Light reflectivity of IPPM and GO.

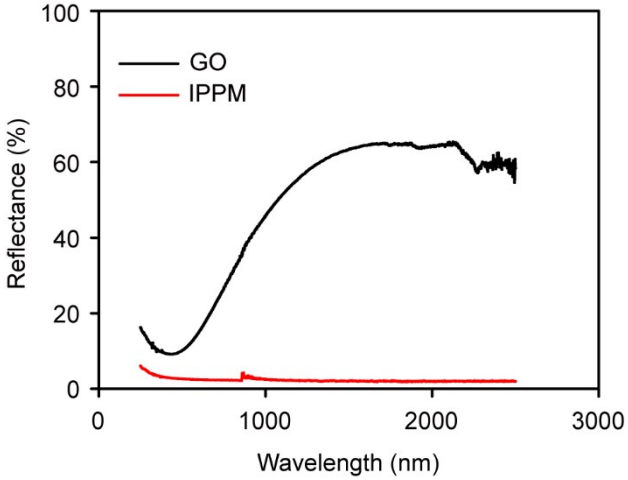

Fig. S8 Light reflectivity of IPPM and GO.

S9. Dark evaporation measurement of IPPM, water and low concentration unlocalized surfactant solutions.

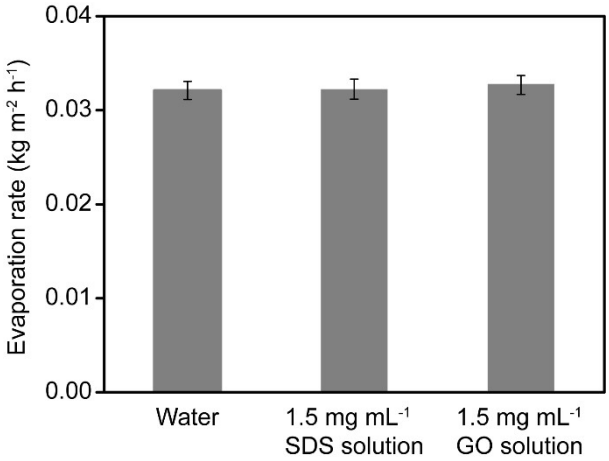

Fig. S9 Comparison of dark evaporation rates of pure water and low concentration unlocalized surfactant solutions.

S10. Models of molecular dynamics simulation.

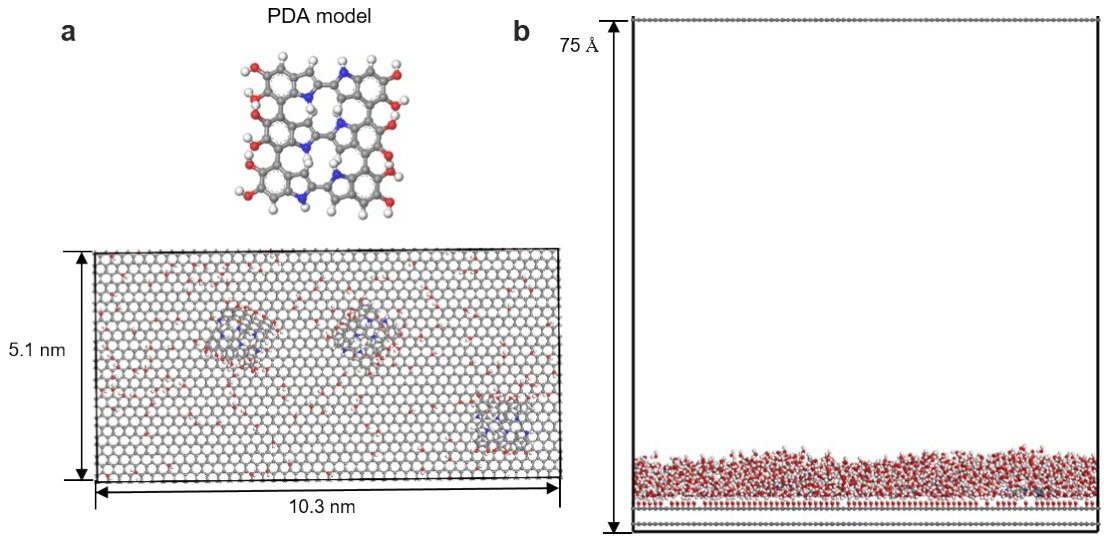

Fig. S10 (a) IPPM model and (b) interfacial interaction model of IPPM and water.

S11. Simulated result of average hydrogen bond length of interfacial water molecules in different systems.

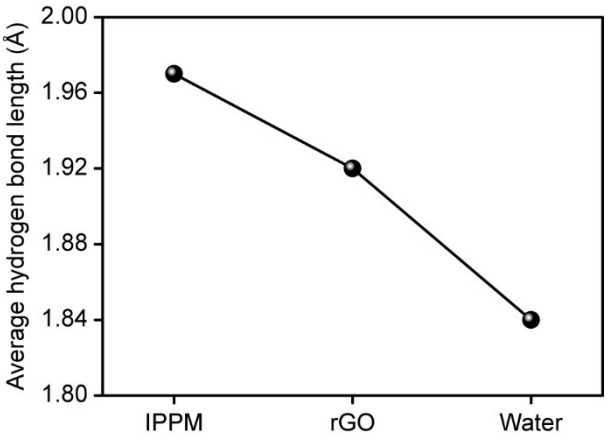

Fig. S11 Average hydrogen bond length of interfacial water molecules in different simulation systems.

S12. Model of quantum chemistry simulation.

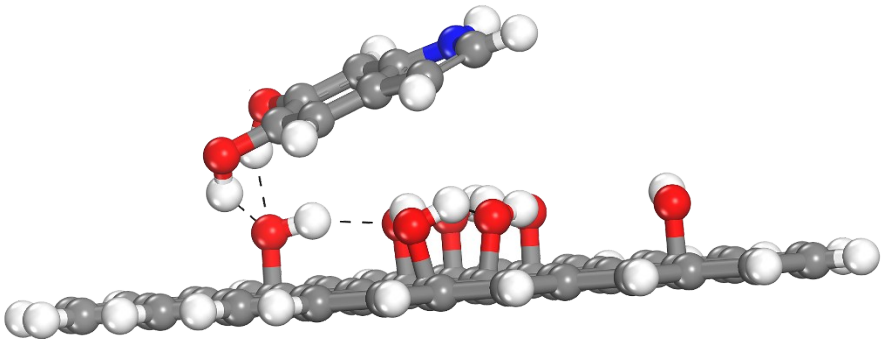

Fig. S12. Simplified rGO & PDA model of quantum chemistry simulation.

S13. Simulated result of the interaction between rGO with different oxygen content and interfacial water molecules.

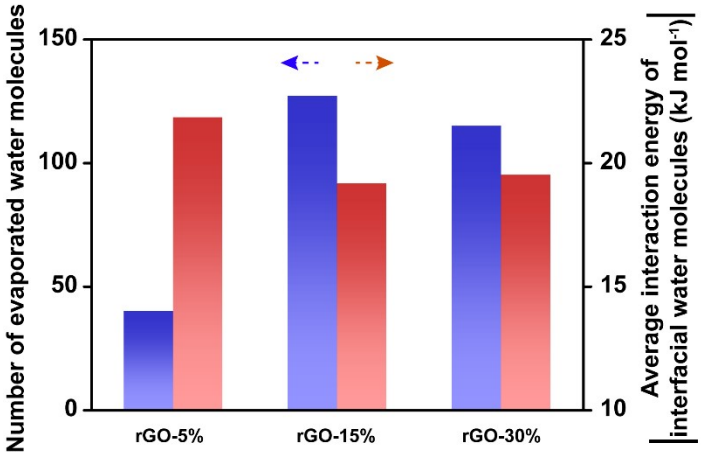

Fig. S13 Number of evaporated water molecules and the absolute value of average interaction energy of interfacial water molecules on the rGO models with different oxygen content.

S14. Solar evaporation system of IPPM

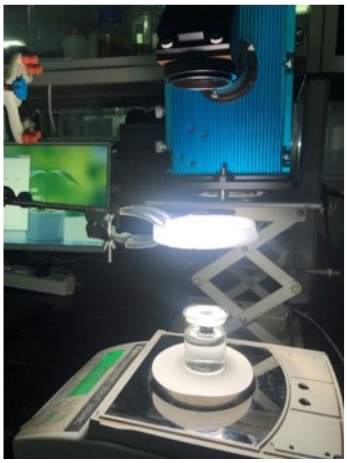

Fig. S14 Photographs of solar evaporation system of IPPM.

S15. SEM images of IPPM-36 h and IPPM-48 h.

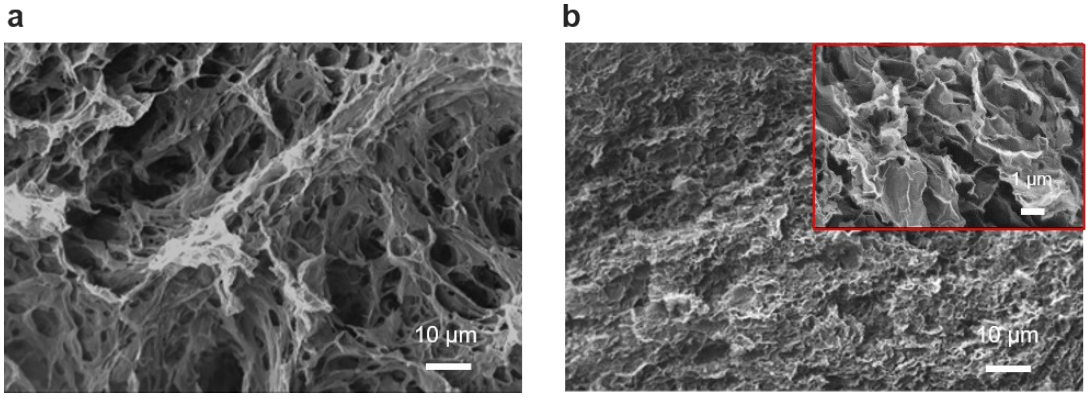

Fig. S15 SEM images of IPPM-36 h and IPPM-48 h.

S16. Dark evaporation rates of IPPM, IPPM-36 h and IPPM-48 h.

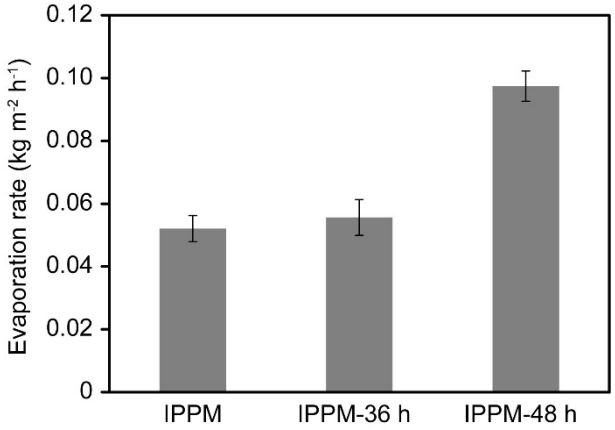

Fig. S16 Dark evaporation rates of IPPM, IPPM-36 h and IPPM-48 h.

S17. Porosities of IPPM, IPPM-36 h, and IPPM-48 h.

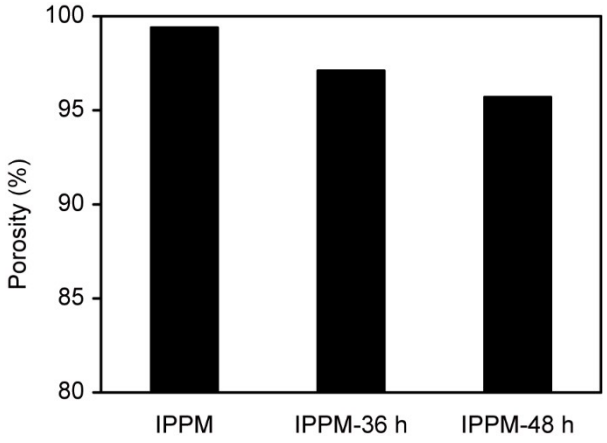

Fig. S17 Porosities of IPPM, IPPM-36 h and IPPM-48 h (obtained by water content test of the samples equivalently).

S18. Water transportability of IPPM, IPPM-36 h, and IPPM-48 h by characterized time-dependent paper wettability test.

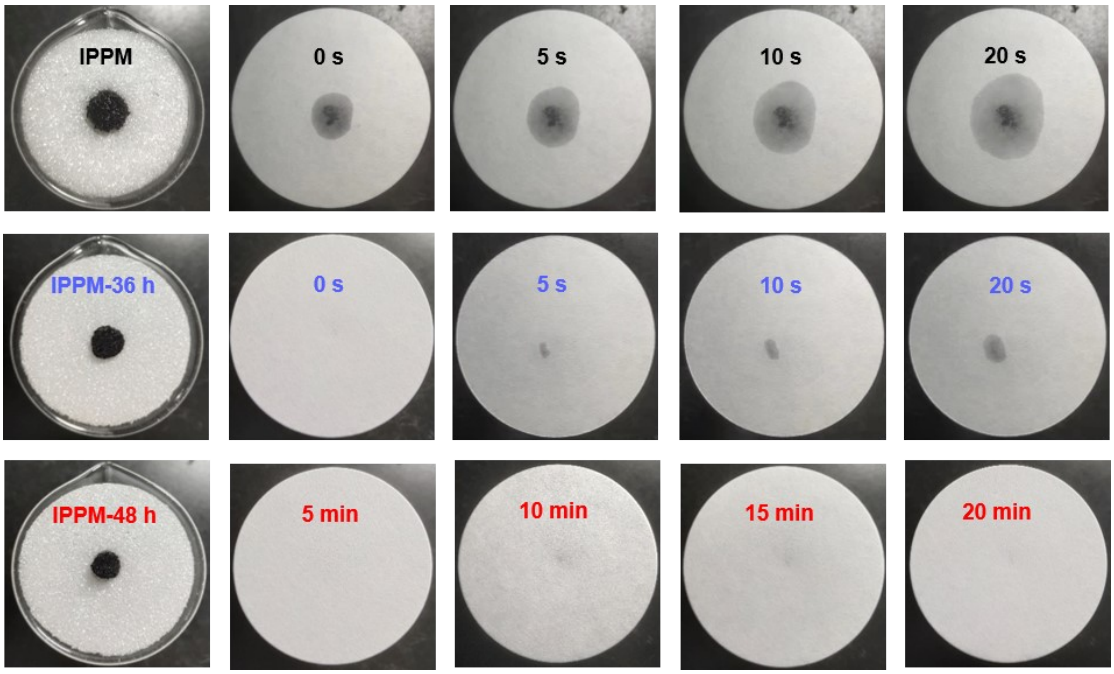

Fig. S18 Water transportability of IPPM, IPPM-36 h, and IPPM-48 h characterized by time-dependent paper wettability test, respectively.

S19. Comsol simulation geometric models for the water transport state in different channel structures.

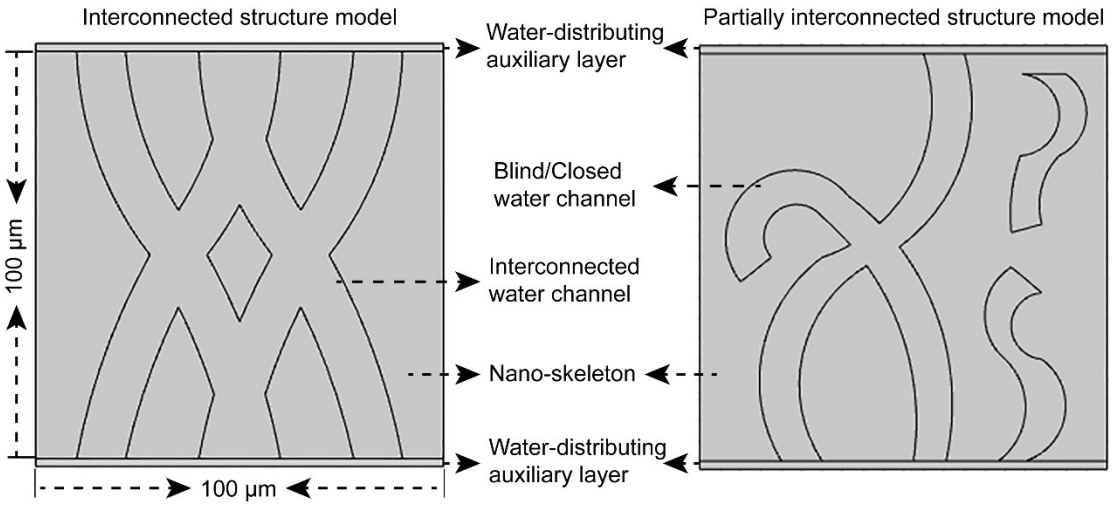

Fig. S19 Geometric models of the interconnected structure in IPPM and partially interconnccected structure in IPPM-48 h.

S20. Photographs of evaporation system for salt solution based on IPPM under high light intensity.

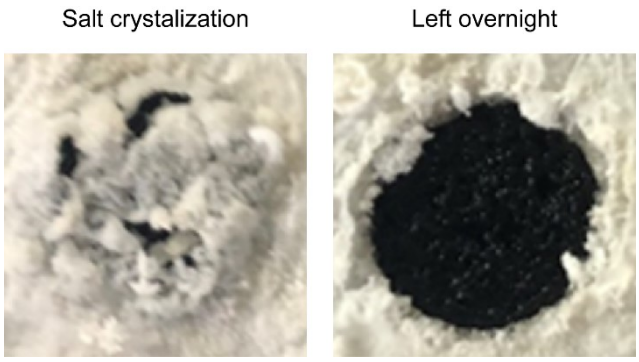

Fig. S20 Photographs of the salt crystallization on the IPPM surface before and after overnight after 8 h evaporation under 5 sun irradiation.

S21. Heavy metal removal measurements.

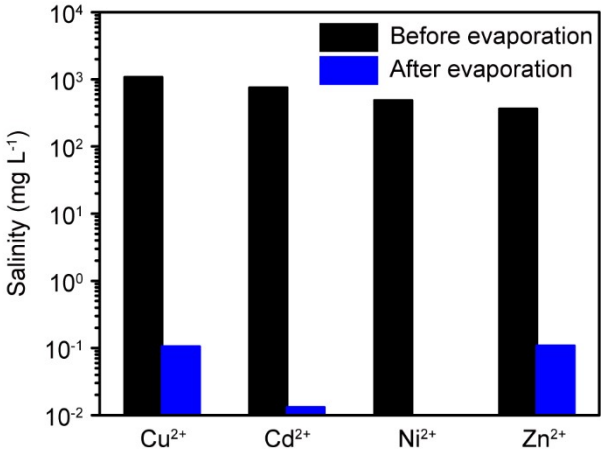

Fig. S21 Heavy metal removal of the evaporation system based on IPPM.